Water Resources Research

RESEARCH ARTICLE
10.1029/2021WR031901

Stability Analysis of Submerged Vegetation Patterns in Rivers

G. Calvani[1], C. Carbonari[1], and L. Solari[1]

[1]Department of Civil and Environmental Engineering, University of Florence, Florence, Italy

Key Points:

- We revised the coupled eco-hydrodynamic problem considering the dynamics of aquatic plants and performed a linear stability analysis
- We modified the equation for vegetation dynamics to account for the removal and resettlement of propagules
- We demonstrated that the resettlement of uprooted propagules is the key process for the onset of vegetation patches

Correspondence to:
G. Calvani,
giulio.calvani@unifi.it

Citation:
Calvani, G., Carbonari, C., & Solari, L. (2022). Stability analysis of submerged vegetation patterns in rivers. *Water Resources Research*, *58*, e2021WR031901. https://doi.org/10.1029/2021WR031901

Received 27 DEC 2021
Accepted 29 JUL 2022

Abstract Aquatic vegetation in fluvial systems is often characterized by spatial patterning of the plant patches. To investigate the conditions for the formation of vegetation patches, we explore the stability of a uniform flow over a non-erodible bed with a uniform vegetation cover of submerged plants. The flow model consists of the two-dimensional shallow water and continuity equations. The hydrodynamic equations are coupled firstly to the classic formulation for vegetation dynamics, and secondly to a modified version of the equation. The revised relationship for vegetation dynamics accounts for the influence of removal, transport, and resettlement of propagules on the growth rate of aquatic vegetation. Linear stability analysis of the eco-hydrodynamic problem is performed by enforcing the quasi-steady approximation. We obtain a dispersion relation disclosing the growth rate and the migration rate of the perturbations of vegetation density as a function of the wavenumber and the relevant flow and vegetation parameters. The present theory predicts the onset of vegetation patterns and includes an adequate wavelength selection mechanism. While uprooting initially reduces plant density, the analysis demonstrates that resettled propagules after removal are fundamental for further plant population increases and the development of vegetation patterns. The proposed framework is then validated against data available in the literature. Additionally, the presence of an upper threshold in terms of vegetation density, above which uniform vegetation cover is stable, might explain the absence of any spatial pattern and thus the extremely dense vegetation cover induced by climate change and invasive species in altered ecosystems.

Plain Language Summary Rivers are complex ecosystems where vegetation plays an important role in shaping the natural habitat. In this work, we study rivers where aquatic plants are present because of favorable conditions for colonization. While vegetation tends to grow and spread, the action exerted by the flow may remove plants, thus reducing the population density. The removed propagules are transported by the flow, may resettle, root and grow, and, in turn, increase the plant density. Starting from an initial riverbed with a uniform vegetation cover, we show that plants tend to arrange themselves into patches with unvegetated gaps between. We perform this analysis through a mathematical approach that allows us to determine the geometrical and dynamic characteristics of the vegetation patterns. These features depend on the value of the relevant hydraulic and plant parameters. Results demonstrate that the production of propagules, together with their resettlement and resprouting, is fundamental for the reproduction of aquatic species and for the development of vegetation patterns. The presence of extremely dense vegetation cover in altered ecosystems due to climate change forcing altering low and high flows and colonization by invasive species is also explained by considering positive feedbacks among plants and the reduction of flow removal.

1. Introduction

The ecological and hydro-morphological significance of aquatic vegetation in lowland rivers is widely acknowledged with aquatic plants providing important habitat for a large number of vertebrates and invertebrates (Corenblit et al., 2007; Gurnell & Grabowski, 2016; Gurnell et al., 2006; O'Hare et al., 2018; Wharton et al., 2006). This results from the interactions between vegetation and flows (Biggs et al., 2019; Cornacchia et al., 2018; Franklin et al., 2008; Marjoribanks et al., 2017) and modification of the transport, trapping and retention of sediment by plants which affects the residence times of sediment-bound nutrients and contaminants (Gurnell & Bertoldi, 2022; Heppell et al., 2009). The interactions may take place at different spatial scales (Schoelynck et al., 2012), from the blade scale, which is key for nutrient uptake by plants, to the patch and reach scales, which are important in sediment transport processes and disturbances induced by flow shear stresses and biogeochemical conditions (Cornacchia et al., 2020; Cotton et al., 2006). Interactions between submerged plants, sediment, and water may affect the growth and decay of plants and the entire morphodynamic evolution of the channel itself (Gurnell, 2014; Gurnell & Grabowski, 2016). As a result of the feedbacks among plants and

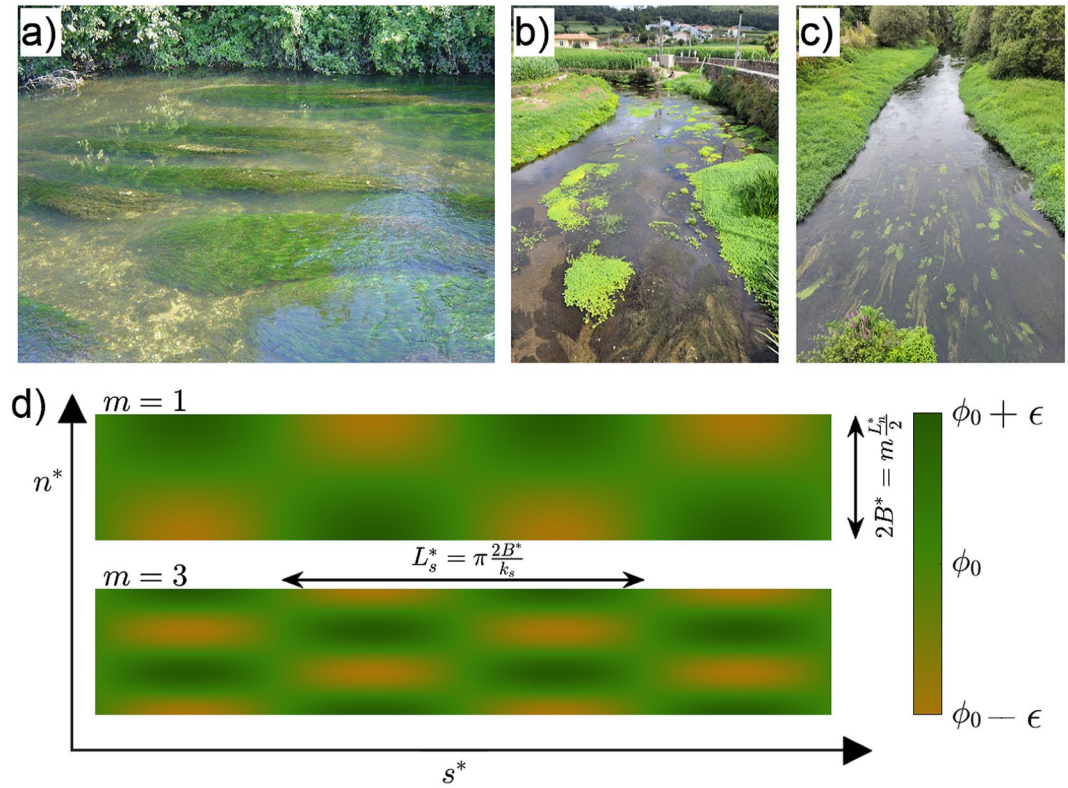

Figure 1. Patterns of vegetation in fluvial environments and sketch of the mathematical model (pictures (b and c) taken by the authors). (a) Lateral view of the River Frome, Dorset (UK) with patches of *Ranunculus* stands (courtesy of Dr. Robert C. Grabowski). (b) Upstream view of the Este River from the San Miguél de Arcos Bridge near Barros, Portugal (Coordinates 41°23'35.38"N 8°40'0.29"W) with patches of emergent and submerged vegetation (July 2021). (c) Upstream view of the Sar River in Padrón, Spain (Coordinates 42°44'20.55"N 8°39'43.48"W) with fully submerged patches (July 2021). (d) Sketch of the mathematical model with dark green and light brown highlighting regions of higher and lower vegetation density, respectively, concerning the equilibrium value, ϕ_0.

between plants and the riverine environment, different patterns of submerged and emergent aquatic vegetation may take place in fluvial ecosystems (Figures 1a–1c), with different morphologies and spatial arrangements of patches (Cornacchia et al., 2018; Larsen & Harvey, 2011; Nepf, 2012).

Organized planform arrangements of vegetation patches are ubiquitous and many studies have reported their presence in different habitats, ranging from grasslands to forests, and from arid systems to savannas and peatlands (Borgogno et al., 2009; Rietkerk et al., 2004, for a review). Several authors analytically investigated the formation of patterns in such environments by considering the action of an external forcing: the dynamics of soil moisture (e.g., Vincenot et al., 2017), the toxicity of dead plants (e.g., Cartenì et al., 2012), the rainfall (e.g., Wang et al., 2017), or the spread of fire (D'Odorico et al., 2007), for instance. Deblauwe et al. (2012), Cartenì et al. (2012), and Bastiaansen et al. (2018), among others, demonstrated that vegetation patterns may migrate, under the influence of external factors. Conversely, some authors showed the formation of self-organized patchiness without the action exerted by forcing. For instance, Lejeune et al. (2004) took into account the balance between cooperative and competitive interactions among different individuals using a diffusion term with a negative coefficient in the equation for vegetation dynamics. And in the absence of external forcing, they also obtained a null value for the migration rate of vegetation patterns. Similar results were obtained by Larsen and Harvey (2011) through a cellular automata model based on simple rules governing the dynamics of vegetation in wetlands subjected to bed elevation changes.

The geometrical characteristics of vegetation patterns in rivers have been analyzed using field investigations (e.g., Cornacchia, Folkard, et al., 2019; Cotton et al., 2006; Schoelynck et al., 2012; Tooth & Nanson, 2000) whereas Gourgue et al. (2021) performed numerical simulations to study the mutual interactions between patterns

Table 1
Parameters and Variables Involved in the Stability Analysis

Symbol	Variable	Value	Units
C_D	Drag coefficient	2	[–]
d^*	Grain size	$1 \cdot 10^{-3}$	m
D_v	Frontal width of plants	0.1	[–]
h_v	Vegetation height	0.75	[–]
k_n	Transverse wavenumber	$\pi/2$	[–]
Y_0^*	Water depth	1	m
α_d^*	Vegetation decay coefficient	$2.04 \cdot 10^{-9}$	m^{-3} s
α_D^*	Vegetation diffusion coefficient	$7.93 \cdot 10^{-8}$	m^2 s^{-1}
α_g^*	Vegetation growth coefficient	$3.17 \cdot 10^{-11}$	m^2 s^{-1}
α_P^*	Propagule coefficient	$2 \cdot 10^{10}$	m^2 s^2

and water flows. Bärenbold et al. (2016) and Crouzy et al. (2016) predicted the critical conditions for the formation of patterns of emergent vegetation based on a stability analysis, a mathematical tool which allows studying the eigenvalues of a problem by simplifying partial differential equations to an algebraic system of linear equations. They both considered emergent riparian plants and a positive value for the diffusion coefficient in the classic logistic law for vegetation dynamics (Camporeale & Ridolfi, 2006). The positive coefficient accounts for positive feedbacks induced by plants on neighboring individuals (D'Odorico et al., 2007). Specifically, the presence of patches of submerged vegetation dampens turbulence and diverts flow, thus creating regions of low flow conditions around and behind the patch itself (Cornacchia, Licci, et al., 2019; Nepf, 2012). This, in turns, creates favorable conditions for the spread of nearby vegetation communities. This process is usually considered to be dependent on the difference between neighboring vegetation densities. Accordingly, it has been typically modeled through a Laplacian operator (2nd order derivative) and a multiplying coefficient governing the dependency between time-derivative and 2nd order spatial-derivative of vegetation density (D'Odorico et al., 2007). The higher the coefficient, the higher the positive sheltering effects, and the higher the positive rate of change in terms of vegetation density. Crouzy et al. (2016) focused on the asymmetry in longitudinal and transverse wavelengths, typically observed in anabranching rivers, while Bärenbold et al. (2016) analyzed patterns of vegetation in single-thread channels. Nonetheless, they both acknowledged the use of extremely high values for vegetated parameters of both growth, decay, and diffusion. As a result, they obtained vegetation dynamics to be faster than water dynamics, and therefore they had to treat the problem by fully coupling the systems of equations.

In this work, we revise and extend the analytical approach of Bärenbold et al. (2016) and Crouzy et al. (2016) to patterns of submerged aquatic vegetation in rivers. First, we demonstrate that the onset of vegetation patterns in fluvial habitats cannot be predicted solely based on the equation for vegetation dynamics. Rather, the onset of patches is governed by the mutual interactions between vegetation and hydrodynamics. Second, we show that the classic logistic law lacks fundamental ingredients to provide acceptable solutions. Finally, we propose a possible solution to overcome such a problem, when vegetation dynamics is considered slower than hydrodynamics (i.e., quasi-steady approximation). The proposed mathematical framework is then validated against data from the literature and the analysis supports the proposed solution, thus showing that vegetation patterns in fluvial ecosystems may arise from propagule dispersal instabilities triggered by hydrodynamic perturbations.

2. Problem Formulation

To highlight the critical conditions for the potential formation of vegetation patterns induced by hydrodynamics only, we adopt the simplest approach to model the interactions between hydraulic and plant dynamics. Thus, we set the conditions of a straight channel with rectangular cross-section and fixed lateral banks, subjected to normal flow conditions, and periodic boundary conditions in the longitudinal direction (i.e., wrapping). The equilibrium state is characterized by a uniform density of plants colonizing the riverbed. We consider the bed not to be erodible (i.e., no erosion or deposition), and we do not account for either sediment transport or changes in bed topography.

Throughout the manuscript, we tackle the problem by involving dimensionless variables. When present, dimensional quantities are denoted by the superscript *. Variables are made dimensionless according to normal flow conditions (indicated by subscript 0) of flow velocity, U_0^*, water depth, Y_0^* and river width, $2B^*$, and the carrying capacity, ϕ_m^*. More specifically, the flow velocity U_0^* is calculated by imposing the value of the Froude number, Fr (i.e., $U_0^* = Fr\sqrt{gY_0^*}$). As an example, we report the dimensionless formula of the vegetation density $\phi = \phi^*/\phi_m^*$. For the relationships of all the dimensionless variables, we address the reader to Appendix A. Values of parameters, as well as dimensional and dimensionless variables, involved in the analysis, are reported in Table 1.

In the following sections, we describe the different approaches involved in the analysis.

2.1. The Classic Equation for Vegetation Dynamics

The equation for vegetation dynamics (Equation 1) in fluvial environments models the evolution in time and space of the plant density. It includes a growth term, whose general solution is represented by a logistic function (Camporeale & Ridolfi, 2006), a decay term due to plant mortality induced by flow uprooting (Perona et al., 2014), and a diffusion term to model positive feedbacks between neighboring vegetation (Bärenbold et al., 2016; Crouzy et al., 2016; D'Odorico et al., 2007). We refer to Equation 1 as the *classic equation* throughout the manuscript to reflect that the formula has been available in the literature for many years (Camporeale & Ridolfi, 2006; D'Odorico et al., 2007). Similarly, we name *classic problem* a system of equations involving Equation 1. The dimensionless form of the classic equation for vegetation dynamics reads:

$$\frac{\partial \phi}{\partial t} = \beta\, \nu_g\, \phi\, (1-\phi) + \frac{\nu_D}{\beta}\, \nabla^2 \phi - \beta\, \nu_d\, \min\{h_v, Y\}\, |\vec{V}|^2\, \phi \tag{1}$$

in which ϕ is the spatial density of vegetation, t is time, β is the width-to-depth ratio (also known as aspect ratio), h_v is the vegetation height, Y is the water depth, $\vec{V} = \{U, V\}$ is the flow velocity, and ν_g, ν_D, and ν_d are the dimensionless parameters for growth, diffusion, and decay, respectively, being α_g^*, α_D^*, and α_d^* their relative dimensional coefficients. Values of vegetation coefficients regarding growth and decay are retrieved from the work of Calvani et al. (2020), whereas the value of the vegetation diffusion coefficient was chosen from the range provided by Sand-Jensen and Madsen (1992). Moreover, the dimensionless vegetation height, h_v, basically represents the relative emergence (analogous to the relative roughness d/Y for sediments with grain size d). Consequently, the term $\min\{h_v, Y\}$ accounts for both submerged ($h_v < Y$) and emergent ($h_v \geq Y$) vegetation. For the sake of simplicity, h_v has already considered the plant reconfiguration induced by flow drag. Therefore, no additional closure relationships are required (Västilä & Järvelä, 2014; Vogel, 1989).

At equilibrium, Equation 1 admits two solutions, one representing barebed conditions ($\phi_{0,2} = 0$), the other uniform vegetation cover ($\phi_{0,1} = 1 - \min\{h_v, 1\}\, \nu_d/\nu_g$). The latter solution was already found by Bärenbold et al. (2016) for emergent vegetation only ($\phi_{0,1} = 1 - \nu_d/\nu_g$). Given the properties of a certain vegetation species (i.e., the growth and decay parameters, ν_g and ν_d, respectively, and the vegetation height, h_v), Calvani et al. (2022) already showed that the solution $\phi_{0,1}$ suggests the existence of a threshold value of the hydrodynamic variables (e.g., Froude number, Fr) for the establishment of that particular vegetation. For the sake of consistency, in the present analysis we consider Froude numbers well below the critical value for the shift toward barebed conditions. In the following, we consider submerged vegetation (i.e., $h_v < 1$) and simply refer to the equilibrium solution as ϕ_0.

A first-order perturbation of Equation 1 is performed by using the mathematical expansion usually adopted in stability analysis (Colombini et al., 1987, among others):

$$\phi = \phi_0 + \epsilon\, (\phi_1\, \exp[\Omega\, t + \boldsymbol{i}\, k_s\, s]\, \sin(k_n\, n) + c.c.) \tag{2}$$

in which the subscript 1 refers to the linear level, ϵ is a small parameter, $\Omega = \Omega_R + \boldsymbol{i}\, \Omega_I$ is the complex wave-speed of the perturbation, s and n are the longitudinal and transverse coordinates, respectively, k_s and k_n are the streamwise and transverse wavenumber (see Figure 1d), respectively, and $c.c$ stands for complex conjugate.

2.2. Stability Analysis of the Eco-Hydrodynamic Problem

We couple the classic equation for submerged vegetation dynamics (Equation 1) with $\min\{h_v, Y\} = h_v$) to the 2D shallow water equations (SWE) for momentum and mass conservation of the water flow. The dimensionless system of equation reads:

$$\frac{\partial U}{\partial t} + U\frac{\partial U}{\partial s} + V\frac{\partial U}{\partial n} + \frac{1}{Fr^2}\left(\frac{\partial Y}{\partial s} - \frac{\partial \eta}{\partial s}\right) + \beta\frac{\tau_s}{Y} = 0 \tag{3}$$

$$\frac{\partial V}{\partial t} + U\frac{\partial V}{\partial s} + V\frac{\partial V}{\partial n} + \frac{1}{Fr^2}\left(\frac{\partial Y}{\partial n} - \frac{\partial \eta}{\partial n}\right) + \beta\frac{\tau_n}{Y} = 0 \tag{4}$$

$$\frac{\partial Y}{\partial t} + \nabla \cdot \left(Y\vec{V}\right) = 0 \tag{5}$$

$$\frac{\partial \phi}{\partial t} - \beta\, \nu_g\, \phi\, (1-\phi) - \frac{\nu_D}{\beta}\, \nabla^2 \phi + \beta\, \nu_d\, h_v\, |\vec{V}|^2\, \phi = 0 \tag{6}$$

We adopt the Chézy formula as closure relationship for the total shear stress $\vec{\tau} = \{\tau_s, \tau_n\} = \frac{|\vec{V}|}{C^2}\{U, V\}$. The total conductance, C, is calculated according to the model of Luhar and Nepf (2013) to account for the presence of submerged vegetation:

$$C = \left(\frac{2}{C_f}\right)^{1/2} \left(1 - \frac{h_v}{Y}\right)^{3/2} + \left(\frac{2}{C_D\, \phi\, h_v\, D_v\, \phi_m}\right)^{1/2} \frac{h_v}{Y} \tag{7}$$

in which $C_f = \left(5.75 \log_{10}\left(2Y_0^*/d^*\right)\right)^{-2}$ is the bed friction coefficient depending on the mean grain size, d^* (Whiting & Dietrich, 1990), C_D is the vegetation drag coefficient, D_v is the frontal width of plants and ϕ_m is the carrying capacity.

We expand hydrodynamic variables in the governing equations at the linear level and adopt a mathematical convenient Ansatz solution (Bärenbold et al., 2016, after Colombini et al., 1987) given by:

$$\{U,\, Y\} = \{U_0,\, Y_0\} + \epsilon\, (\{U_1,\, Y_1\}\, \exp\left[\Omega\, t + \boldsymbol{i}\, k_s\, s\right]\, \sin\left(k_n\, n\right) + c.c.) \tag{8}$$

$$V = V_0 + \epsilon\, (V_1\, \exp\left[\Omega\, t + \boldsymbol{i}\, k_s\, s\right]\, \cos\left(k_n\, n\right) + c.c.) \tag{9}$$

being $\{U_0,\, V_0,\, Y_0,\, \phi_0\} = \{1,\, 0,\, 1,\, 1 - h_v\, \nu_d/\nu_g\}$ the solution at the leading order (i.e., normal flow conditions with uniform vegetation density). The transverse wavenumber, k_n, must assume multiple values of $\pi/2$ due to the lateral boundary conditions imposed at the riverbanks (i.e., $k_n = m\pi/2$). For the sake of simplicity, we assume $m = 1$ to model the onset of alternate patterns of vegetation (see Figure 1d), without loss of generality of the main purposes of this work. For vegetation patterns characterized by multiple patches in the same cross section (e.g., $m = 2$ or $m = 3$), we address the reader to the analysis of Carbonari et al. (2022) and to the work of Crosato and Mosselman (2009) for an analogy to sediment bars.

The values of vegetation coefficients involved in the analysis (Table 1) and the corresponding dimensionless parameters (e.g., ν_g) imply that vegetation dynamics ($O(10^{-8} - 10^{-6})$) is much slower than hydrodynamics ($O(1)$). Such hypothesis allows for the quasi-steady approximation in Equations 3–5, similarly to what it is usually done in the stability analysis of morphodynamics (i.e., water-sediment interactions) (Colombini & Carbonari, 2020; Colombini & Stocchino, 2012; Colombini et al., 1987, among others). By involving Equations 2, 8, and 9 and by applying the quasi-steady approximation, the system of Equations 3–6 can be turned into an algebraic system with complex coefficients:

$$\begin{pmatrix} \boldsymbol{i} k_s + 2\frac{\beta}{C_0^2} & 0 & \frac{\boldsymbol{i} k_s}{Fr^2} - \frac{2\beta C_{1,Y} + \beta C_0}{C_0^3} & -2C_{1,\phi}\, \frac{\beta}{C_0^3} \\ 0 & \boldsymbol{i} k_s + \frac{\beta}{C_0^2} & \frac{k_n}{Fr^2} & 0 \\ \boldsymbol{i} k_s & -k_n & \boldsymbol{i} k_s & 0 \\ 2\, \beta\, \nu_d\, h_v\, \phi_0 & 0 & 0 & \beta \nu_g \phi_0 + \frac{\nu_D}{\beta}\left(k_s^2 + k_n^2\right) + \Omega \end{pmatrix} \begin{pmatrix} U_1 \\ V_1 \\ Y_1 \\ \phi_1 \end{pmatrix} = \begin{pmatrix} 0 \\ 0 \\ 0 \\ 0 \end{pmatrix} \tag{10}$$

in which the complex wave-speed Ω is the eigenvalue of the vegetation dynamics. In the system, C_0 is the Chézy coefficient (Equation 7) and $C_{1,Y} = \left.\frac{\partial C}{\partial Y}\right|_0$ and $C_{1,\phi} = \left.\frac{\partial C}{\partial \phi}\right|_0$ are its partial derivatives in Y and ϕ, respectively. The subscript 0 indicates that the three terms are evaluated at the base state (that is, $Y = Y_0,\ \phi = \phi_0$).

The characteristic polynomial, also known as the dispersion relation, of the square matrix in Equation 10 is a simple linear equation in Ω. Its solution provides the growth (i.e., amplification) rate, Ω_R, and migration rate (i.e., celerity), Ω_I, of the perturbation. The analysis of Ω_R's sign determines whether vegetation patterns may show up ($\Omega_R > 0$) or not ($\Omega_R \leq 0$).

2.3. A Modified Version of the Classic Model

The growth of vegetation density depends on the deposition and establishment of vegetative propagules, generated by flow induced breakage or uprooting (Gurnell et al., 2007). Propagules are transported downstream within the water column or floating on the water surface before settling (Eckert et al., 2016; Gurnell et al., 2008; Heidbüchel et al., 2020; Nilsson et al., 2010). In the classic equation (Equation 1), such processes are intrinsically modeled by the vegetation growth rate, ν_g. However, no influence of propagule transport or deposition is present in the formulation, as the parameter ν_g is constant. We model the change of the vegetation growth rate by accounting for the propagules produced by the process of plant decay and/or breakage and their transport and settlement. The proposed equations reads:

$$\frac{\partial \phi}{\partial t} = \beta\, \nu_g\, \phi\, (1-\phi)\left(1 - \frac{\nu_P}{\beta\,(\nu_g\, \phi_0\, (1-\phi_0))^2}\, \nabla \cdot \left[\nu_d\, h_v\, \phi\, |\vec{V}|^2\, \vec{V}\right]\right) + \\ + \frac{\nu_D}{\beta}\, \nabla^2 \phi - \beta\, \nu_d\, h_v |\vec{V}|^2\, \phi \tag{11}$$

in which the quantity $\nu_d\, h_v\, \phi\, |\vec{V}|^2$ resembles the decay rate of vegetation and thereby represents the production of propagules and velocity vector, $\vec{V}$, accounts for spatial-heterogeneity in the velocity field. Consequently, the divergence term considers the variations both in the transport of propagules within the control volume due to main flow diversion and in the spatial production of propagules due to uprooting or breakage (Eckert et al., 2016; Heidbüchel et al., 2020). The parameter ν_P models the influence of propagule production, transport, and settlement on the vegetation growth rate through the coefficient α_P^*.

Similarly to the classic version of the equation for vegetation dynamics (Equation 1), the proposed formulation (Equation 11) is coupled to SWE for hydrodynamics. The system is then perturbed and the same Ansatz solutions are involved for the governing variables (Equations 2, 8, and 9). The problem at the linear level remains unchanged in the first three lines of thesystem Equation 10. Equation 4 (i.e., vegetation dynamics) is updated as follows:

$$(2\,\beta\,\nu_d\,h_v\,\phi_0 + 3\nu_P \boldsymbol{i} k_s)\; U_1 - \nu_P k_n\, V_1 + \left(\beta\,\nu_g\,\phi_0 + \frac{\nu_D}{\beta}\left(k_s^2 + k_n^2\right) + \frac{\nu_P}{\phi_0}\boldsymbol{i} k_s + \Omega\right)\phi_1 = 0 \tag{12}$$

For the sake of simplicity, we consider values of the parameter ν_P in the same range of the other parameters for vegetation dynamics (e.g., $10^{-8} - 10^{-6}$), as no studies provided values for such a quantity. Additionally, ν_P values of similar order of magnitude of the other vegetation parameters ensures that the different terms of Equation 12 have the same relevance. Having one of the parameters much smaller than the others implies that the process governed by such a parameter is negligible. Under this assumption, the quasi-steady approximation is still valid for the algebraic problem, and the characteristic polynomial remains a simple linear relation in the variable Ω.

3. Results

3.1. Stability Analysis of the Classic Equation

First, we demonstrate that the equation for vegetation dynamics (Equation 1) cannot predict the onset of vegetation patterns on its own. We recall that the diffusive term models the spread of vegetation from areas with higher plant density to neighboring regions with lower plant density (i.e., positive feedbacks between plants). Such spread depends on the cooperative interactions between plants in the two areas and, as such, it implies the positive value of the diffusion coefficient, ν_D, according to D'Odorico et al. (2007). By substituting Equation 2 in Equation 1, we obtain a solution for the complex wave speed Ω, whose real part, Ω_R, and the imaginary part, Ω_I, represent the growth rate and the migration rate of the perturbation, respectively. The solution reads:

$$\Omega_R + \boldsymbol{i}\,\Omega_I = -\beta\,\nu_g\,\phi_0 \; - \; \frac{\nu_D}{\beta}\left(k_s^2 + k_n^2\right) \tag{13}$$

in which the right-hand side term is a linear expression in the variable ν_D with real coefficients. This implies that Ω_I is null and, as a consequence, potential vegetation patterns do not migrate. The formation of patterns occurs

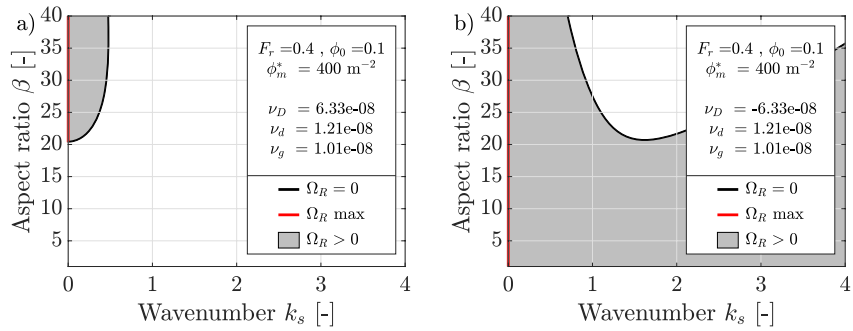

Figure 2. Stability plots of the eco-hydrodynamic problem (Equation 10) with the classic equation for vegetation dynamics (Equation 1) by varying the diffusion coefficient, ν_D. Gray regions highlight a positive growth rate. Maximum amplification is shown by the red curve. Values of fixed variables and parameters are indicated in Table 1 or shown in the legend box. (a) Stability plot with positive diffusion coefficient ($\nu_D > 0$); (b) Stability plot with negative diffusion coefficient ($\nu_D < 0$).

when the real quantity Ω_R is strictly positive. Accordingly, the simple mathematics in Equation 13 leads to the condition

$$\nu_D < -\frac{\beta^2\ \nu_g\ \phi_0}{k_s^2 + k_n^2} \tag{14}$$

Given that the fraction on the right-hand side is a positive and real quantity, the diffusion coefficient must assume negative values to allow for the formation of vegetation patterns. This result contradicts the original hypothesis of positive feedbacks (Crouzy et al., 2016; D'Odorico et al., 2007). On the contrary, if one accounts for a negative diffusion coefficient to model, for instance, negative feedbacks among plants due to erosion induced by flow acceleration between patches (e.g., Meire et al., 2014; van Wesenbeeck et al., 2008), the solution of the marginal curve (i.e., $\Omega_R = 0$) from Equation 13 reads

$$\beta = \sqrt{\frac{-\nu_D}{\nu_g\ \phi_0}}k_s + \sqrt{\frac{-\nu_D}{\nu_g\ \phi_0}\ k_n^2} \tag{15}$$

which represents a straight line in the $k_s - \beta$ space. The threshold condition for instability toward patterns is represented by the minimum value of β, which occurs for $k_s = 0$. This means that vegetation patterns have no longitudinal wavelength, which seems counter-intuitive if compared to the patterns of Figure 1 showing observed spatial patterns of submerged aquatic vegetation observed from field surveys and reported in the literature (Cornacchia et al., 2020; Schoelynck et al., 2012; Wharton et al., 2006, among others).

Consequently, the formation of vegetation patterns may be predicted by the equation for plant dynamics only when it is coupled to additional relationships modeling external forcing (e.g., Cartenì et al., 2012; Vincenot et al., 2017; Wang et al., 2017). In the following, we consider the instability induced by hydrodynamic forces, similar to Bärenbold et al. (2016) and Crouzy et al. (2016).

3.2. Stability Analysis of the Classic Eco-Hydrodynamic Problem

The characteristic polynomial of the system of Equations 10 is herein solved, providing the eigenvalue Ω. The real part of the eigenvalue, Ω_R, is investigated by varying the aspect ratio, β, and the longitudinal wavenumber, k_s, and by setting values for the other variables (see Table 1). Particularly, regarding the diffusive coefficient ν_D, both positive and negative values are involved in the analysis. Results of the analysis are graphically represented in Figure 2, where the so-called stability plot identifies regions of positive (i.e., growing unstable perturbations) and negative values of Ω_R. The regions of positive and negative amplification rate are separated by the marginal curve (thick black line in Figure 3) and it is noteworthy that the marginal curve graphically represents the relationship $\Omega_R = 0$. The $k_s - \beta$ space has been chosen to represent the results, analogous to sediment bars in 2D morphodynamic problems (Colombini et al., 1987, among others) and similar to previous works dealing with stability analysis of vegetation patterns (Bärenbold et al., 2016; Crouzy et al., 2016).

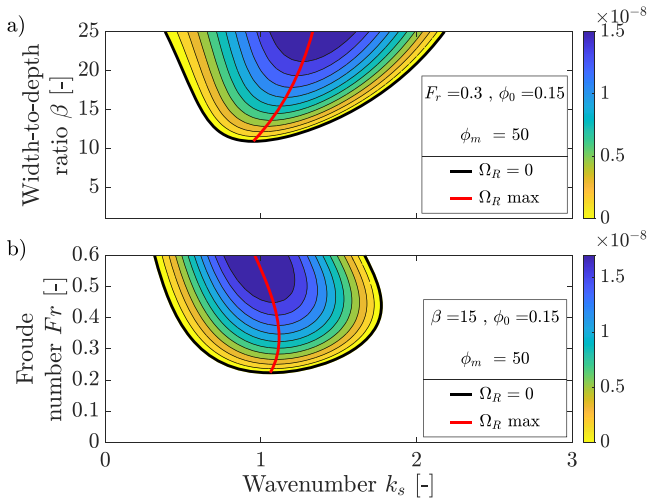

Figure 3. Stability plots for the modified eco-hydrodynamic problem. Colored regions are associated with $\Omega_R > 0$, white regions with $\Omega_R < 0$, marginal curve is indicated by the thick black line, maximum amplification by red line. Values of fixed variables and parameters are listed. (a) The stability plot in the $k_s - \beta$ parameter space; (b) The stability plot in the $k_s - Fr$ parameter space.

Figure 2a shows the stability plot of Ω_R for the positive value of the diffusion coefficient, ν_D. The marginal curve ($\Omega_R = 0$) identifies a region of positive amplification rate above a certain threshold of the aspect ratio, β, while the most unstable wavenumber (maximum growth rate) is highlighted by the red curve. Such a curve shows that the growth rate assumes maximum values corresponding to the y-axis, represented by the value $k_s = 0$.

For comparison, Figure 2b shows the marginal curve for the same hydraulic conditions (e.g., Froude number) and vegetation parameters of Figure 2a, but the diffusion coefficient takes the opposite value. The analysis of the classic equation (Equation 15) suggests that instability toward patterns may arise by accounting for negative feedbacks (i.e., negative diffusion coefficient). In this case, we explore the implications related to the approach adopted by Lejeune et al. (2004). Nevertheless, coupling the equation to SWE (Figure 2b) shows that instability occurs for a broad range of longitudinal wavenumber, k_s, being the unstable region ($\Omega_R > 0$) indefinitely unbounded toward high values of k_s. Additionally, the marginal curve does not show a threshold value of the aspect ratio, β, and instability occurs for low values of the aspect ratio (e.g., $\beta \approx 1$). Lastly, the most unstable wavenumber again overlaps the y-axis (i.e., $k_s = 0$), similar to the stability plot in Figure 2a. We anticipate that such results are analytically meaningless, and we address the reader to the Discussion section for further remarks on the significance of maximum growth rate occurring at $k_s = 0$.

3.3. Stability Analysis of the Modified Eco-Hydrodynamic Problem

Similar to Equation 1, the modified equation for vegetation dynamics (Equation 11) does not allow for the formation of patterns of vegetation, when we refer to this equation alone. This can be simply demonstrated by considering that the real part of the term containing phi_1 is the same both in the system at the linear level (compare fourth line in Equation 10 and Equation 12). The phi_1 term containing the imaginary unit in Equation 12 contributes to the imaginary part (i.e., celerity, Ω_I) of the eigenvalue, Ω, and not to the growth rate, Ω_R. For the sake of simplicity and in line with previous studies (Bärenbold et al., 2016; Crouzy et al., 2016; D'Odorico et al., 2007), we consider a positive diffusion coefficient in the modified relationship for vegetation dynamics.

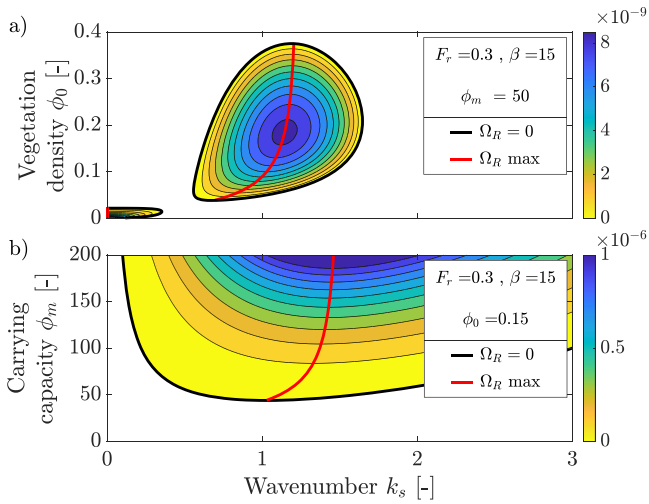

Figure 4. Stability plots for the modified eco-hydrodynamic problem. Colored regions are associated with $\Omega_R > 0$, white regions with $\Omega_R < 0$, marginal curve is indicated by the thick black line, maximum amplification by red line. Values of fixed variables and parameters are listed. (a) The stability plot in the $k_s - \phi_0$ parameter space; (b) The stability plot in the $k_s - \phi_m$ parameter space.

The linear problem formed by the first three lines of the system Equation 10 coupled with Equation 12 basically differs from the classic eco-hydrodynamic problem (system Equation 10) in the terms related to U_1 and V_1 and in the term $ik_s \nu_P/\phi_0$ associated to ϕ_1. The solution of the linear problem (i.e., the eigenvalue Ω) is therefore revised, as well as the resulting stability scenarios.

The main results of the analysis are illustrated using several stability plots (Figures 3 and 4), where the behavior of the amplification rate, Ω_R, is investigated in the framework of different parameter spaces. The main dimensionless parameters involved in the analysis are reported in the legend of each plot. Global coefficients are reported in Table 1. For clarification, vegetation parameters (e.g., ν_g and ν_d) may change according to the framework of the stability plots, mainly because they depend on Froude number, Fr, equilibrium vegetation density, ϕ_0, and carrying capacity, ϕ_m^*. For this reason, they are constant in the $k_s - \beta$ space, only. In the other stability plots, their values vary in line with the formulations provided in Appendix A. Thus, when vegetation parameters vary, we perform the analysis by modifying the decay coefficient, α_d^*, and by keeping the growth coefficient, α_g^*, and the vegetation equilibrium density, ϕ_0, constant.

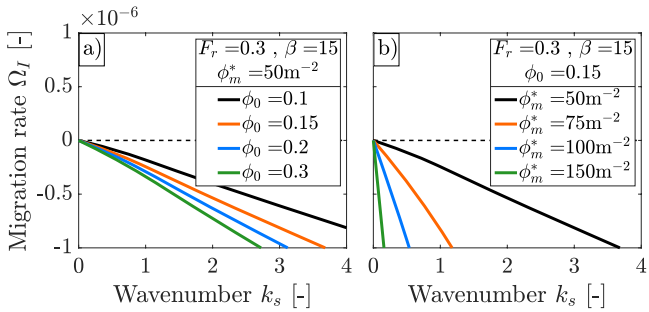

Figure 5. The trend of the migrations rate, Ω_I, versus the longitudinal wavenumber, k_s at varying vegetation characteristics. Main vegetation and flow properties are reported in Table 1. (a) Ω_I for some values of the initial vegetation density, ϕ_0; (b) Ω_I for some values of the carrying capacity, ϕ_m.

In each plot, isolines (thin black lines) identify points with equal growth rates, Ω_R. The marginal curve (thick black line) divides the parameter space into regions of positive and negative growth rate. The white area is associated with stable uniform vegetation density in the space-time domain (i.e., $\Omega_R < 0$). The colored region is associated with unstable perturbation acting on vegetation density leading to vegetation pattern formation (i.e., $\Omega_R > 0$). As indicated by the color bar, positive growth rate values increase from light warm to dark cool colors. The red line indicates the wavenumber of maximum amplification. For a given condition (the quantity on the y-axis), the presence of a unique wavenumber indicated by the red curve demonstrates that a selection mechanism is adequately included in the analysis and this is essential for the meaningfulness of the results.

Figures 3a and 3b shows the stability plot in the $k_s - \beta$ and in the $k_s - Fr$ parameter space, respectively. Both the stability plots in Figure 3 illustrate a distinct unstable region in the corresponding parameter space. For the range of β plotted in Figure 3a, the maximum growth rate (red curve) occurs for values of k_s in the range 0.95–1.35, whereas in Figure 3b the maximum amplification occurs in a narrower range of k_s ($0.96 \leq k_s \leq 1.12$). A critical threshold above which vegetation patterns start to develop is visible in both the panels: for the values of parameters involved in the analysis, this is equal to $\beta = 10.9$ and $Fr = 0.22$, respectively.

Figure 4a illustrates the stability plot in the $k_s - \phi_0$ parameter space. Using ϕ_0 as a variable means that the initial vegetation density varies according to the selected value on the y-axis but it is constant within the river reach. Figure 4b shows the stability plot in the $k_s - \phi_m$ parameter space. The latter panel displays a single unstable region, whereas the analysis in the $k_s - \phi_0$ reveals that an unstable region exists near the origin of the axis, for the very low value of the initial equilibrium density. Both the panels in Figure 4 show the selection mechanism of the wavenumber k_s: for the values of parameters involved in the analysis (Table 1), it occurs for $0.72 \leq k_s \leq 1.2$ in the $k_s - \phi_0$ space and for $1.05 \leq k_s \leq 1.46$ in the $k_s - \phi_m$ space. The threshold for the onset of vegetation patterns is unambiguously identifiable in Figure 4b ($\phi_m \geq 44$), whereas Figure 4a shows that the threshold value is $\phi_0 = 0$. However, for a more likely value of the initial vegetation density, a second threshold can be identified as $\phi_0 \geq 0.025$. Interestingly, a further critical value ($\phi_0 = 0.38$) limits the unstable region in the upper part of the stability plot.

At the linear level, the coupled eco-hydrodynamic problem with the modified equation for vegetation dynamics (Equation 12) presents a term proportional to V_1 and a complex coefficient in U_1. Conversely, in the classic coupled problem (Equation 10), they are null and real, respectively. The combination of these terms with the rest of the coefficients strongly affects the characteristic polynomial of the system. Such terms modify the overall balance between stabilizing and destabilizing effects, and, as a consequence, the overall behavior of the eigenvalue, both in the real (Figures 3, 4, and 6c) and in the imaginary parts. Particularly, it is worth mentioning that our analysis may capture the main features of the migration rate, Ω_I, of the emerging vegetation patches.

The analysis of the imaginary part of the eigenvalue, Ω_I, provides information on the dynamics of the patches of vegetation by revealing how fast the vegetation patterns may migrate within the channel. Figure 5 illustrates the migration rate as a function of the wavenumber for the values of Fr, β, ϕ_m, and ϕ_0 reported in the legend of each panel. For those values, we have already shown the onset of vegetation patches in Figure 4. In this regard, we explore the celerity of such patterns in Figure 5. According to the classical approach for river bar morphodynamics (Colombini et al., 1987), positive $\Omega_I > 0$ corresponds to the upstream migration of the patterns, whereas negative values indicate that perturbations migrate downstream.

3.4. Validation and Practical Application

We apply the proposed framework to a river reach of the River Frome (UK). The Frome Vauchurch reach (see Figure 1) is a groundwater-fed, chalk stream, characterized by the presence of macrophyte cover, mostly *Ranunculus penicillatus*. The presence of patterns of submerged vegetation patches is reported by many authors (Cornacchia et al., 2020; Cotton et al., 2006; Watson, 2007; Wharton et al., 2006, among others). For the sake of

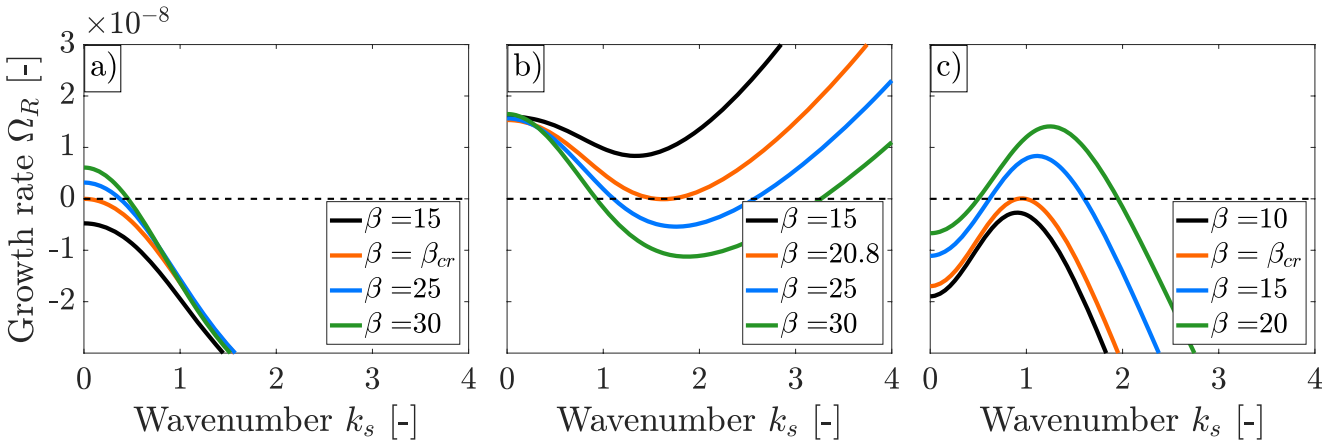

Figure 6. Comparison between growth rates of the coupled eco-hydrodynamic problems according to different formulation of the equation for vegetation dynamics at varying the parameter β. (a) Growth rate trends for the classic equation (Equation 1) with positive diffusion coefficient, ν_D (see Figure 2a for parameter values); (b) Growth rate trends for the classic equation (Equation 1) with negative diffusion coefficient, ν_D (see Figure 2b for parameter values); (c) Growth rate trends for the modified equation (Equation 11) accounting for propagule resettlement (see Figure 3a for parameter values).

model validation, we compare the predicted longitudinal wavenumber, k_s, corresponding to the maximum amplification rate (red lines in Figures 3 and 4 to the measures of patch lengths provided by Watson (2007).

Data of flow conditions, water depth, and river characteristics (e.g., mean river width, $2B^* = 8.9$ m) were retrieved from Cornacchia et al. (2020) according to similar values of the Froude number, Fr. Vegetation is characterized by the presence of multiple patches within the cross-section (e.g., $m = 3$), $h_v = 0.9$ to account for almost emergent conditions, and carrying capacity $\phi_m^* = 200$ m^{-2} as reported by the authors (Cornacchia et al., 2020). We consider growth and diffusion coefficients as reported in Table 1 whereas the decay coefficient is calculated by imposing $\phi_0 = 0.15$. Watson (2007) reported an average pattern length, L_s^*, of 4.5 m, corresponding to a longitudinal wavenumber $k_s = 2\pi B^*/L_s^* = 6.2$. By accounting for a 10% tolerance in the measurements (i.e., $L_s^* = 4.5 \pm 0.45$ m), the patch wavenumber lies in the range $k_s = 5.65$–6.90. We consider the same tolerance for the predicted wavenumbers. Table 2 reports the predicted values at the maximum growth rate and the corresponding range based on 0.45 m tolerance.

Table 2
Predicted Wavenumbers of Vegetation Patches in the River Frome (Figure 1a)

Fr	β	k_s (Ω_R max)	k_s range
0.05	9.27	5.46	5.02–5.98
	10.6	5.81	5.32–6.41
0.1	8.90	6.35	5.76–7.07
	10.9	5.90	5.39–6.52
	11.1	6.72	6.07–7.54
	12.7	5.58	5.12–6.13
0.15	8.90	6.11	5.57–6.78
	10.3	5.72	5.23–6.29
	11.0	6.01	5.48–6.65
	13.1	6.27	5.70–6.98
	13.5	5.67	5.19–6.24
	14.8	5.41	4.97–5.92
0.2	9.08	5.71	5.23–6.28
	9.18	5.54	5.09–6.09
	10.9	5.30	4.89–5.80
	13.5	5.11	4.72–5.57

Note. All values are dimensionless. Measured range is $k_s = 5.65$–6.90 (Watson, 2007).

The predicted range of wavenumbers overlaps the measured quantities for most of the provided data. The model better performs for measurements with $Fr = 0.10$ and $Fr = 0.15$, whereas for $Fr = 0.05$ and $Fr = 0.20$ the predicted range of wavenumbers has a general tendency to underestimate the measured values. Only in one case ($Fr = 0.2$ and $\beta = 13.5$), the predicted range lies just outside the measured one (maximum predicted $k_s = 5.57$, minimum measured wavenumber $k_s = 5.65$). In terms of wavelength, such discrepancy corresponds to 0.07 m in a measured wavelength $L_s^* = 4.5$ m (1.6% error).

The proposed mathematical framework may be involved in practical applications aiming at improving the heterogeneity of fluvial environments. For given hydrological characteristics (e.g., average discharge, Q), sediment size (i.e., mean grain diameter, d_{50}^*) of the river reach, and for given plant species and properties (e.g., growth, α_g^*, and diffusion, α_D^*, coefficients), the river width may be adjusted to obtain a width-to-depth ratio, β, higher than the threshold value, β_c (see Figure 3a). As a result, the formation of patches is promoted. Conversely, one may also proceed in the opposite direction, by narrowing the river reach to limit the value of the width-to-depth ratio below the threshold value, thus preventing the development of patches. Similarly,

for a given aspect ratio occurring in the river reach under restoration, one may select the plant species with the characteristics to allow or inhibit the formation of patterns.

4. Discussion

4.1. The Classic Equation for Vegetation Dynamics

The classic equation for vegetation dynamics (Equation 1) admits a solution toward vegetation patterns for negative values of the diffusion coefficient, ν_D. This approach was used by Lejeune et al. (2004), among others, to analyze the onset of vegetation patterns in arid ecosystems. Despite the use of a different equation for vegetation dynamics, which was further expanded by additional non-linear terms (e.g., ϕ^3 and $\nabla^4\phi$), the authors demonstrated that the negative diffusion coefficient is the only term responsible for a positive growth rate of the perturbation. In this respect, the condition imposed by Equation 14 agrees with the results of Lejeune et al. (2004). Interestingly, the presence of the cubic term (i.e., ϕ^3) leads to the development of an upper threshold limit in the $k_s - \phi_0$ space, similar to the stability plot in Figure 4a. However, Lejeune et al. (2004) did not clarify what ϕ^3 was supposed to model. For the case of fluvial environments, we demonstrated (Equation 15) that considering the equation for vegetation dynamics only predicts the onset of patterns with infinite longitudinal wavelength (i.e., $k_s = 0$). These patterns resembling stripes rather than alternate patches are commonly found in dry and wetlands (Cheng et al., 2011; Larsen & Harvey, 2011; Lejeune et al., 2004) but they have never been reported in rivers (e.g., Cornacchia et al., 2018; Schoelynck et al., 2012; Watson, 2007; Wharton et al., 2006). Furthermore, it is remarkable to note that Lejeune et al. (2004) obtained a null value for the migration rate, Ω_l, due to the absence of external forcing.

As a general remark, the decay term in the equation models the vegetation mortality induced by flow drag. The decay process does not account for scouring and erosion processes promoting uprooting (Type II uprooting, according to Edmaier et al. (2011)). Therefore, the influence of sediment dynamics on flow-induced mortality is only embedded in the decay parameter, ν_d (Bärenbold et al., 2016; Calvani et al., 2020; Perona et al., 2014). Additionally, the decay term does not distinguish between different processes of plant loss (e.g., breakage or uprooting), although both the processes depend on the flow drag acting on the plant surface $\left(\propto h_v\,|\vec{V}|^2\right)$. Thus, further research must be carried out (e.g., Cornacchia et al., 2020; Riis & Biggs, 2003; Schoelynck et al., 2012).

4.2. Coupled Eco-Hydrodynamic Problem With the Classic Equation

The classic eco-hydrodynamic problem shows the same issue as the previous analysis, as already mentioned when presenting the results in Figure 2. The presence of a threshold in the aspect ratio, Figure 2a, is acknowledged when stability analysis is performed. Although this threshold has similar characteristics to the critical conditions for the occurrence of bedforms (i.e., bars and dunes in gravel-bed and sand-bed rivers, respectively), the overall results of the analysis reported in Figure 2a are difficult to interpret. We already showed that the maximum value of the growth rate takes place along the y-axis (red line in Figure 2a), that is $k_s = 0$ (Figure 6a). Again, this condition corresponds to the onset of longitudinal vegetation stripes as opposed to patches of finite length.

A possible solution to the coupled eco-hydrodynamic problem was found by Bärenbold et al. (2016) and Crouzy et al. (2016). Although involving high values of the vegetation parameters, as well as the full unsteadiness of the SWE, seems a reasonable approach to solve the problem of vegetation patterns, we think that the onset of instability must be proved by accounting for realistic values of plant parameters. In the light of our results (Figure 2), coupling the classic equation for vegetation dynamics to SWE does not predict the critical conditions for the formation of vegetation patterns. Even the use of a negative diffusion coefficient (Equation 14) does not provide satisfactory results (Figure 6b). More specifically, Figure 2b demonstrates that the coupled eco-hydrodynamic problem with a negative diffusion coefficient shows that the maximum amplification rate once again takes place for $k_s = 0$. In this case, the results are meaningless because even the initial equilibrium configuration (i.e., $k_s = k_n = 0$) is unstable and no threshold value (i.e., $\beta = 0$) limits the unstable region, which appears to be unbounded toward infinite values of the wavenumber, k_s.

Our analysis demonstrates that the classic equation for vegetation dynamics in rivers lacks some ingredients necessary to capture the onset of instability toward patterns of finite length. To overcome the issue, we have introduced a new, physically meaningful, term in Equation 11 to account for the positive effects induced by propagules

on the growth rate of submerged aquatic vegetation. Results have shown that such a term may induce instability in the eigenvalue problem (Figures 3 and 4). In this context, Figure 6c shows that the growth rate, Ω_R, is positive for values of width-to-depth ratio higher than a threshold ($\beta > \beta_c$) and remains positive in a certain range of the wavenumber, k_s.

4.3. Coupled Eco-Hydrodynamic Problem With the Modified Equation

The proposed equation for vegetation dynamics accounts for the transport, settling and sprouting of removed propagules due to flow uprooting or breakage (Equation 11). This propagation mechanism has been proved fundamental for submerged aquatic vegetation, whereas riparian plants mostly reproduce via seed dispersal (see Barrat-Segretain, 1996, for a review).

The proposed approach seems to provide promising results (see Figures 3 and 4) and the validation against field data turned out satisfactory (Table 2), with only one case with predicted wavenumbers outside the measured range. We tackled the problem by keeping the mathematical model as simple and physically-based as possible. To further deepen the analysis and consider additional aspects, one may take into account nutrient transport and morphodynamic-related processes. Nutrient transport may be introduced by considering turbulent fluctuations and molecular diffusion with a more refined flow model (e.g., fully 3D hydrodynamic equations). Regarding sediment processes, a negative diffusion coefficient can be incorporated into the proposed Equation 11 to account for negative feedbacks due to erosion at patch edges (e.g., Meire et al., 2014; van Wesenbeeck et al., 2008). However, this approach, as demonstrated in this manuscript, may lead to unsatisfactory results. It must be also considered that the diffusion term is represented by the Laplacian of the vegetation density (Equations 1 and 11) and not of the bed elevation, that the hypothesis behind the negative coefficient would suggest. According to this consideration, a proper term ($\propto \nabla^2 \eta$) may be included in the equation and account for bed elevation changes (Exner equation). In this regard, Bärenbold et al. (2016) have already proved the presence of morphodynamic processes to affect the shape and characteristics (e.g., threshold aspect ratio) of marginal curves.

Flow diversion induced by the presence of discrete vegetation patches may be introduced in the hydrodynamic equations (i.e., in the continuity equation (Equation 5) for highly vegetated riverbeds. For the values of parameters and vegetation density used in the present analysis, the vegetated volume fraction represents less than 0.1% of the volume domain. For this purpose, it is worth noting that the stability plot in Figure 4a shows that it exists an upper threshold ($\phi_0 = 0.38$) for the onset of vegetation patterns. In correspondence with such threshold value and for the vegetation and hydraulic characteristics (Table 1), the vegetated volume fraction is equal to 0.22%, a value which does not justify the use of a more complicated mass-conservation equation.

Here we report a sensitivity analysis performed on some of the coefficients involved in the analysis. We considered six different variables, namely the drag coefficient, C_D, the frontal width of plants, D_v, the Chézy coefficient, C_0 and the growth, α_g^*, the decay, α_d^*, and the diffusion, α_D^*, coefficients. To allow for comparison with the stability plot in Figure 3a, the results of the analysis are reported in terms of the threshold aspect ratio, β_c. We considered β_c because the aspect ratio is usually acknowledged to play a role in 2D shallow-water systems. For example, it governs the emergence of bar patterns and the morphodynamic evolution of multiple thread channels (e.g., Colombini et al., 1987; Crosato & Mosselman, 2009), and was previously used to analyze the onset of vegetation patterns (Bärenbold et al., 2016; Crouzy et al., 2016). We must also point out that the results of the sensitivity analysis may be meaningless when the threshold aspect ratio takes very low values (i.e., $\beta_c \approx 1$). In this case, the 2D SWE (Equations 3–5) cannot be applied and the mathematical framework loses its reliability.

Figure 7 shows results of the sensitivity analysis, according to different coefficients and parameters for some values of the Froude number, Fr. The analysis indicates that the decay and diffusion coefficients play the major role in selecting the threshold aspect ratio, β_c, for a wide range of values of the Froude number, Fr (Figures 7e and 7f). The growth coefficient, α_g^*, seems relevant for all the tested hydraulic conditions (i.e., Froude number) for values lower than 0.7×10^{-10} m^2 s^{-1} (Figure 7d), whereas its influence on β_c becomes negligible for higher values. The model is responsive to the Chézy coefficient, C_0, for values higher than 6 and Froude number higher than 2 (Figure 7c), whereas the threshold aspect ratio, β_c, significantly varies for Froude number equal to 0.1. The trend is similar for other variables (e.g., drag coefficient, C_D, in Figure 7a and plant width, D_v, in Figure 7b). It is noteworthy that the dependence of the threshold aspect ratio, β_c, on the drag coefficient, C_D, and the frontal width of plants, D_v, is almost linear and decreases at increasing values of the Froude number, Fr. This may suggest that

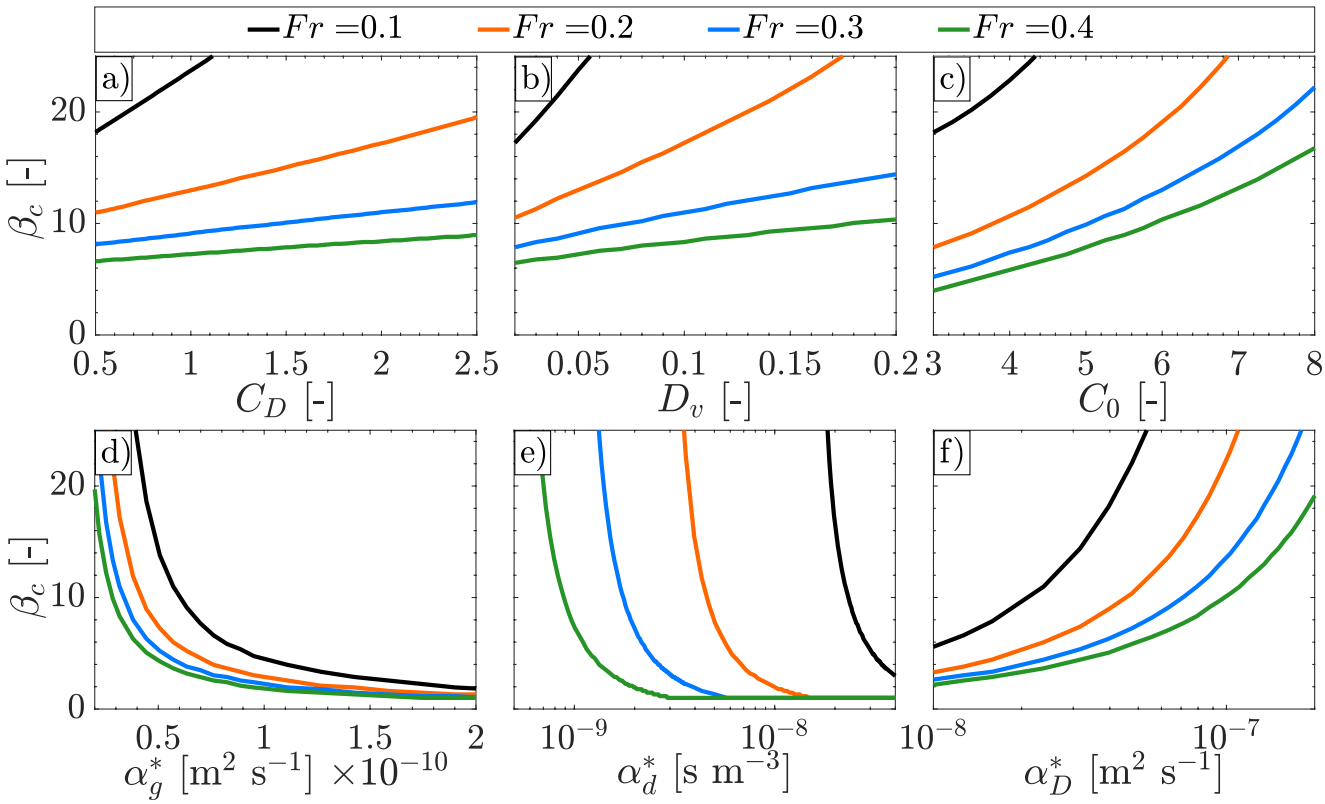

Figure 7. Sensitivity analysis of the threshold aspect ratio, β_c, with respect to different coefficients involved in the model (Equations 7, 11, and 12). (a) β_c versus the drag coefficient, C_D; (b) β_c versus the frontal width of plants, D_v; (c) β_c versus the Chézy coefficient, C_0; (d) β_c versus the growth coefficient, α_g^*; (e) β_c versus the decay coefficient, α_d^*; (f) β_c versus the diffusion coefficient, α_D^*.

vegetation patches may show up at high values of the Froude number (higher than the 0.3 in the proposed framework) according to the parameters governing vegetation dynamics (e.g., α_g^*) rather than those related to plant geometry (e.g., D_v) and plant-scale turbulence (e.g., C_D).

The presence of an upper threshold in terms of vegetation density, ϕ_0, in Figure 4a implies that vegetation density remains constant and uniform above such threshold. Besides the role played by other factors (e.g., thermal alterations, nutrient availability), the existence of such an upper threshold may explain the development of vegetation cover by invasive species. The positive feedbacks induced by high vegetation cover (e.g., reduction of plant removal and breakage due to low flow velocities in the vegetated layer) may promote the increase in vegetation density up to extremely high values. This may take place to such a point that plant removal is physically impeded by the very low flow drag, and patterns may not come up. The hampered formation of vegetation patterns due to high vegetation density is consistent with field observations which give evidence to the uniform and dense vegetation cover of invasive species (e.g., Ibáñez et al., 2012; Thamaga & Dube, 2018). In these cases, human interventions are mandatory to recover and restore fluvial and ecological equilibrium (Rahel et al., 2008, among others).

According to the values of parameters involved in the analysis, the magnitude of Ω_I (Figure 5) is similar to the range measured by Deblauwe et al. (2012) for the migration of banded vegetation patterns in arid ecosystems but the values in the range are much lower than the migration rate of morphological bedforms (e.g., Rodrigues et al., 2015; Serlet et al., 2018). Additionally, Figure 5 reveals that Ω_I assumes negative values, only, meaning that vegetation patterns may migrate under the influence of the hydrodynamic forcing, but only in the downstream direction. These results are in contrast to the measurements of Deblauwe et al. (2012) and Bastiaansen et al. (2018), where patterns migrate upslope, and to the findings of Cartenì et al. (2012), where patterns migrate both in the upstream and in the downstream directions. To this regard, we must point out that all the aforementioned papers did not deal with hydrodynamic interactions as they were meant to model vegetation patterns in

drylands and arid ecosystems. Moreover, Cartenì et al. (2012) assumed a system of spatial coordinates with no slope and no preferred direction, which may explain the occurrence of the migration in both directions.

5. Conclusions

In this work, we revised the coupled eco-hydrodynamic problem to shed light on the threshold conditions for the formation of vegetation patterns of aquatic plants in rivers. The mathematical approach is based on the linear stability analysis of a modified equation modeling vegetation dynamics in terms of plant density. The proposed formulation accounts for the positive feedbacks induced by the removal of propagules on the growth rate of the plants. We proved that the onset of vegetation patches from a uniform vegetated riverbed may be explained by the transport and resettlement of uprooted or broken propagules (Eckert et al., 2016; Heidbüchel et al., 2020).

Both the onset of vegetation patterns and their geometrical characteristics depend on the hydrodynamic parameters (e.g., Froude number) and the specific plant-species properties (e.g., growth, diffusion, decay coefficients). As a consequence, the management of vegetated rivers is challenging in particular due to the hydrological effects of climate change, the impacts of land use practices on sediment dynamics, and the presence of invasive species. The results of our analysis may explain the formation of extremely dense vegetation covers when non-native species start colonizing the riverbed. The proposed framework also represents a valid tool for informing the design of river restoration projects. Vegetation patches play a key role aiming at improving in the physical and biological diversity of lowland permeable rivers including the management of low and high flows.

Appendix A: Dimensionless Variables

In this appendix, we report the mathematical expression of dimensionless variables.

$$D_v = D_v^*/Y_0^* \tag{A1}$$

$$h_v = h_v^*/Y_0^* \tag{A2}$$

$$n = n^*/B^* \tag{A3}$$

$$s = s^*/B^* \tag{A4}$$

$$t = t^* \frac{U_0^*}{B^*} \tag{A5}$$

$$U = U^*/U_0^* \tag{A6}$$

$$V = V^*/U_0^* \tag{A7}$$

$$Y = Y^*/Y_0^* \tag{A8}$$

$$\beta = B^*/Y_0^* \tag{A9}$$

$$\nu_d = \alpha_d^* \, Y_0^{*5/2} \, Fr \, g^{1/2} \tag{A10}$$

$$\nu_D = \alpha_D^* \, Y_0^{*-3/2} \, Fr^{-1} \, g^{-1/2} \tag{A11}$$

$$\nu_g = \alpha_g^* \, \phi_m^* \, Y_0^{*1/2} \, Fr^{-1} \, g^{-1/2} \tag{A12}$$

$$\nu_P = \alpha_P^* \, \nu_d \, \nu_g \, \phi_0^2 \, (1-\phi_0) \, \phi_m^* \, h_v \, U_0^{*2} \, Y_0^{*-2} \tag{A13}$$

$$\phi = \phi^* \, / \, \phi_m^* \tag{A14}$$

$$\phi_m = \phi_m^* \, Y_0^{*2} \tag{A15}$$

Notation

C_{D}	Drag coefficient
C_f	Bed friction coefficient
$d*$	Grain size
D_v	Frontal width of plants
Fr	Froude number
g	Acceleration due to gravity
h_{v}	Vegetation height
k_n	Transverse wavenumber
k_s	Longitudinal wavenumber
L_s^*	Longitudinal wavelength
n	Transverse coordinate
s	Longitudinal coordinate
t	Time
U	Longitudinal flow velocity
V	Transverse flow velocity
$\overrightarrow{V} = \{U, V\}$	Flow velocity vector
Y	Water depth
α_d^*	Vegetation decay coefficient
α_D^*	Vegetation diffusion coefficient
α_g^*	Vegetation growth coefficient
α_P^*	Propagule coefficient
β	Width-to-depth ratio
β_c	Threshold width-to-depth ratio
ϵ	Small number
η	Bed elevation
ν_d	Vegetation decay parameter
ν_D	Vegetation diffusion parameter
ν_g	Vegetation growth parameter
ν_P	Propagule parameter
$\overrightarrow{\tau} = \{\tau_s, \tau_n\}$	Bed shear stress
ϕ	Vegetation density
ϕ_0	Vegetation density at equilibrium
ϕ_m	Carrying capacity
ϕ_m^*	Dimensional carrying capacity
$\Omega = \Omega_R + i\Omega_I$	Complex wave-speed of the perturbation

Data Availability Statement

Data used in the analysis are reported in the tables and within the text.

Acknowledgments
The authors are thankful to Marco Colombini and Duccio Fanelli for fruitful discussion on the proposed model. The authors express a special thank to Geraldene Wharton for both the enlightening discussion on patch dynamics and the language polishing. The authors wish to thank the Associate Editor and three anonymous Reviewers for their comments on the first and second draft of the manuscript.

References

Bärenbold, F., Crouzy, B., & Perona, P. (2016). Stability analysis of ecomorphodynamic equations. *Water Resources Research*, *52*(2), 1070–1088. https://doi.org/10.1002/2015wr017492

Barrat-Segretain, M. (1996). Strategies of reproduction, dispersion, and competition in river plants: A review. *Vegetatio*, *123*(1), 13–37. https://doi.org/10.1007/bf00044885

Bastiaansen, R., Jaïbi, O., Deblauwe, V., Eppinga, M. B., Siteur, K., Siero, E., et al. (2018). Multistability of model and real dryland ecosystems through spatial self-organization. *Proceedings of the National Academy of Sciences of the United States of America*, *115*(44), 11256–11261. https://doi.org/10.1073/pnas.1804771115

Biggs, H. J., Nikora, V., Gibbins, C., Cameron, S., Papadopoulos, K., Stewart, M., et al. (2019). Flow interactions with an aquatic macrophyte: A field study using stereoscopic particle image velocimetry. *Journal of Ecohydraulics*, *4*(2), 113–130. https://doi.org/10.1080/24705357.2019.1606677

Borgogno, F., D'Odorico, P., Laio, F., & Ridolfi, L. (2009). Mathematical models of vegetation pattern formation in ecohydrology. *Reviews of Geophysics*, *47*(1), RG1005. https://doi.org/10.1029/2007rg000256

Calvani, G., Carbonari, C., & Solari, L. (2022). Threshold conditions for the shift between vegetated and barebed rivers. *Geophysical Research Letters*, *49*(1), e2021GL096393. https://doi.org/10.1029/2021gl096393

Calvani, G., Perona, P., Schick, C., & Solari, L. (2020). Biomorphological scaling laws from convectively accelerated streams. *Earth Surface Processes and Landforms*, *45*(3), 723–735. https://doi.org/10.1002/esp.4735

Camporeale, C., & Ridolfi, L. (2006). Riparian vegetation distribution induced by river flow variability: A stochastic approach. *Water Resources Research*, *42*(10), W10415. https://doi.org/10.1029/2006wr004933

Carbonari, C., Calvani, G., & Solari, L. (2022). Explaining multiple patches of aquatic vegetation through linear stability analysis. *Environmental Fluid Mechanics*, *1–14*(2–3), 645–658. https://doi.org/10.1007/s10652-022-09843-8

Cartenì, F., Marasco, A., Bonanomi, G., Mazzoleni, S., Rietkerk, M., & Giannino, F. (2012). Negative plant soil feedback explaining ring formation in clonal plants. *Journal of Theoretical Biology*, *313*, 153–161. https://doi.org/10.1016/j.jtbi.2012.08.008

Cheng, Y., Stieglitz, M., Turk, G., & Engel, V. (2011). Effects of anisotropy on pattern formation in wetland ecosystems. *Geophysical Research Letters*, *38*(4), L04402. https://doi.org/10.1029/2010gl046091

Colombini, M., & Carbonari, C. (2020). Sorting and bed waves in unidirectional shallow-water flows. *Journal of Fluid Mechanics*, *885*, A46. https://doi.org/10.1017/jfm.2019.1039

Colombini, M., Seminara, G., & Tubino, M. (1987). Finite-amplitude alternate bars. *Journal of Fluid Mechanics*, *181*, 213–232. https://doi.org/10.1017/s0022112087002064

Colombini, M., & Stocchino, A. (2012). Three-dimensional river bed forms. *Journal of Fluid Mechanics*, *695*, 63–80. https://doi.org/10.1017/jfm.2011.556

Corenblit, D., Tabacchi, E., Steiger, J., & Gurnell, A. M. (2007). Reciprocal interactions and adjustments between fluvial landforms and vegetation dynamics in river corridors: A review of complementary approaches. *Earth-Science Reviews*, *84*(1–2), 56–86. https://doi.org/10.1016/j.earscirev.2007.05.004

Cornacchia, L., Folkard, A., Davies, G., Grabowski, R. C., van de Koppel, J., van der Wal, D., et al. (2019). Plants face the flow in V formation: A study of plant patch alignment in streams. *Limnology & Oceanography*, *64*(3), 1087–1102. https://doi.org/10.1002/lno.11099

Cornacchia, L., Licci, S., Nepf, H., Folkard, A., van der Wal, D., van de Koppel, J., et al. (2019). Turbulence-mediated facilitation of resource uptake in patchy stream macrophytes. *Limnology & Oceanography*, *64*(2), 714–727. https://doi.org/10.1002/lno.11070

Cornacchia, L., van de Koppel, J., van der Wal, D., Wharton, G., Puijalon, S., & Bouma, T. J. (2018). Landscapes of facilitation: How self-organized patchiness of aquatic macrophytes promotes diversity in streams. *Ecology*, *99*(4), 832–847. https://doi.org/10.1002/ecy.2177

Cornacchia, L., Wharton, G., Davies, G., Grabowski, R. C., Temmerman, S., Van Der Wal, D., et al. (2020). Self-organization of river vegetation leads to emergent buffering of river flows and water levels. *Proceedings of the Royal Society B*, *287*(1931), 20201147. https://doi.org/10.1098/rspb.2020.1147

Cotton, J., Wharton, G., Bass, J., Heppell, C., & Wotton, R. (2006). The effects of seasonal changes to in-stream vegetation cover on patterns of flow and accumulation of sediment. *Geomorphology*, *77*(3–4), 320–334. https://doi.org/10.1016/j.geomorph.2006.01.010

Crosato, A., & Mosselman, E. (2009). Simple physics-based predictor for the number of river bars and the transition between meandering and braiding. *Water Resources Research*, *45*(3), W03424. https://doi.org/10.1029/2008wr007242

Crouzy, B., Bärenbold, F., D'Odorico, P., & Perona, P. (2016). Ecomorphodynamic approaches to river anabranching patterns. *Advances in Water Resources*, *93*, 156–165. https://doi.org/10.1016/j.advwatres.2015.07.011

D'Odorico, P., Laio, F., Porporato, A., Ridolfi, L., & Barbier, N. (2007). Noise-induced vegetation patterns in fire-prone savannas. *Journal of Geophysical Research*, *112*(G2), G02021. https://doi.org/10.1029/2006jg000261

Deblauwe, V., Couteron, P., Bogaert, J., & Barbier, N. (2012). Determinants and dynamics of banded vegetation pattern migration in arid climates. *Ecological Monographs*, *82*(1), 3–21. https://doi.org/10.1890/11-0362.1

Eckert, C. G., Dorken, M. E., & Barrett, S. C. (2016). Ecological and evolutionary consequences of sexual and clonal reproduction in aquatic plants. *Aquatic Botany*, *135*, 46–61. https://doi.org/10.1016/j.aquabot.2016.03.006

Edmaier, K., Burlando, P., & Perona, P. (2011). Mechanisms of vegetation uprooting by flow in alluvial non-cohesive sediment. *Hydrology and Earth System Sciences*, *15*(5), 1615–1627. https://doi.org/10.5194/hess-15-1615-2011

Franklin, P., Dunbar, M., & Whitehead, P. (2008). Flow controls on lowland river macrophytes: A review. *Science of the Total Environment*, *400*(1), 369–378. https://doi.org/10.1016/j.scitotenv.2008.06.018

Gourgue, O., van Belzen, J., Schwarz, C., Bouma, T. J., van de Koppel, J., & Temmerman, S. (2021). A convolution method to assess subgrid-scale interactions between flow and patchy vegetation in biogeomorphic models. *Journal of Advances in Modeling Earth Systems*, *13*(2), e2020MS002116. https://doi.org/10.1029/2020ms002116

Gurnell, A. (2014). Plants as river system engineers. *Earth Surface Processes and Landforms*, *39*(1), 4–25. https://doi.org/10.1002/esp.3397

Gurnell, A., & Bertoldi, W. (2022). The impact of plants on fine sediment storage within the active channels of gravel-bed rivers: A preliminary assessment. *Hydrological Processes*, *36*(7), e14637. https://doi.org/10.1002/hyp.14637

Gurnell, A., Goodson, J., Thompson, K., Clifford, N., & Armitage, P. (2007). The river-Bed: A dynamic store for plant propagules? *Earth Surface Processes and Landforms*, *32*(8), 1257–1272. https://doi.org/10.1002/esp.1554

Gurnell, A., & Grabowski, R. C. (2016). Vegetation–hydrogeomorphology interactions in a low-energy, human-impacted river. *River Research and Applications*, *32*(2), 202–215. https://doi.org/10.1002/rra.2922

Gurnell, A., Thompson, K., Goodson, J., & Moggridge, H. (2008). Propagule deposition along river margins: Linking hydrology and ecology. *Journal of Ecology*, *96*(3), 553–565. https://doi.org/10.1111/j.1365-2745.2008.01358.x

Gurnell, A., van Oosterhout, M. P., de Vlieger, B., & Goodson, J. M. (2006). Reach-scale interactions between aquatic plants and physical habitat: River Frome, Dorset. *River Research and Applications*, *22*(6), 667–680. https://doi.org/10.1002/rra.929

Heidbüchel, P., Sachs, M., Hamzehian, N., & Hussner, A. (2020). Go with the flow: Fragment retention patterns shape the vegetative dispersal of aquatic plants in lowland streams. *Freshwater Biology*, *65*(11), 1936–1949. https://doi.org/10.1111/fwb.13590

Heppell, C., Wharton, G., Cotton, J., Bass, J., & Roberts, S. (2009). Sediment storage in the shallow hyporheic of lowland vegetated river reaches. *Hydrological Processes: An International Journal*, *23*(15), 2239–2251. https://doi.org/10.1002/hyp.7283

Ibáñez, C., Alcaraz, C., Caiola, N., Rovira, A., Trobajo, R., Alonso, M., et al. (2012). Regime shift from phytoplankton to macrophyte dominance in a large river: Top-down versus bottom-up effects. *Science of the Total Environment*, *416*, 314–322. https://doi.org/10.1016/j.scitotenv.2011.11.059

Larsen, L. G., & Harvey, J. W. (2011). Modeling of hydroecological feedbacks predicts distinct classes of landscape pattern, process, and restoration potential in shallow aquatic ecosystems. *Geomorphology*, *126*(3), 279–296. (Geomorphology on Multiscale Feedbacks in Ecogeomorphology). https://doi.org/10.1016/j.geomorph.2010.03.015

Lejeune, O., Tlidi, M., & Lefever, R. (2004). Vegetation spots and stripes: Dissipative structures in arid landscapes. *International Journal of Quantum Chemistry*, *98*(2), 261–271. https://doi.org/10.1002/qua.10878

Luhar, M., & Nepf, H. M. (2013). From the blade scale to the reach scale: A characterization of aquatic vegetative drag. *Advances in Water Resources*, *51*, 305–316. https://doi.org/10.1016/j.advwatres.2012.02.002

Marjoribanks, T. I., Hardy, R. J., Lane, S. N., & Tancock, M. J. (2017). Patch-scale representation of vegetation within hydraulic models. *Earth Surface Processes and Landforms*, *42*(5), 699–710. https://doi.org/10.1002/esp.4015

Meire, D. W., Kondziolka, J. M., & Nepf, H. M. (2014). Interaction between neighboring vegetation patches: Impact on flow and deposition. *Water Resources Research*, *50*(5), 3809–3825. https://doi.org/10.1002/2013wr015070

Nepf, H. M. (2012). Flow and transport in regions with aquatic vegetation. *Annual Review of Fluid Mechanics*, *44*(1), 123–142. https://doi.org/10.1146/annurev-fluid-120710-101048

Nilsson, C., Brown, R. L., Jansson, R., & Merritt, D. M. (2010). The role of hydrochory in structuring riparian and wetland vegetation. *Biological Reviews*, *85*(4), 837–858. https://doi.org/10.1111/j.1469-185x.2010.00129.x

O'Hare, M. T., Aguiar, F. C., Asaeda, T., Bakker, E. S., Chambers, P. A., Clayton, J. S., et al. (2018). Plants in aquatic ecosystems: Current trends and future directions. *Hydrobiologia*, *812*(1), 1–11. https://doi.org/10.1007/s10750-017-3190-7

Perona, P., Crouzy, B., McLelland, S., Molnar, P., & Camporeale, C. (2014). Ecomorphodynamics of rivers with converging boundaries. *Earth Surface Processes and Landforms*, *39*(12), 1651–1662. https://doi.org/10.1002/esp.3614

Rahel, F. J., Bierwagen, B., & Taniguchi, Y. (2008). Managing aquatic species of conservation concern in the face of climate change and invasive species. *Conservation Biology*, *22*(3), 551–561. https://doi.org/10.1111/j.1523-1739.2008.00953.x

Rietkerk, M., Dekker, S. C., De Ruiter, P. C., & van de Koppel, J. (2004). Self-organized patchiness and catastrophic shifts in ecosystems. *Science*, *305*(5692), 1926–1929. https://doi.org/10.1126/science.1101867

Riis, T., & Biggs, B. J. F. (2003). Hydrologic and hydraulic control of macrophyte establishment and performance in streams. *Limnology & Oceanography*, *48*(4), 1488–1497. https://doi.org/10.4319/lo.2003.48.4.1488

Rodrigues, S., Mosselman, E., Claude, N., Wintenberger, C. L., & Juge, P. (2015). Alternate bars in a sandy gravel bed river: Generation, migration and interactions with superimposed dunes. *Earth Surface Processes and Landforms*, *40*(5), 610–628. https://doi.org/10.1002/esp.3657

Sand-Jensen, K., & Madsen, T. V. (1992). Patch dynamics of the stream macrophyte, callitriche cophocarpa. *Freshwater Biology*, *27*(2), 277–282. https://doi.org/10.1111/j.1365-2427.1992.tb00539.x

Schoelynck, J., de Groote, T., Bal, K., Vandenbruwaene, W., Meire, P., & Temmerman, S. (2012). Self-organised patchiness and scale-dependent bio-geomorphic feedbacks in aquatic river vegetation. *Ecography*, *35*(8), 760–768. https://doi.org/10.1111/j.1600-0587.2011.07177.x

Serlet, A. J., Gurnell, A. M., Zolezzi, G., Wharton, G., Belleudy, P., & Jourdain, C. (2018). Biomorphodynamics of alternate bars in a channelized, regulated river: An integrated historical and modelling analysis. *Earth Surface Processes and Landforms*, *43*(9), 1739–1756. https://doi.org/10.1002/esp.4349

Thamaga, K. H., & Dube, T. (2018). Remote sensing of invasive water hyacinth (Eichhornia crassipes): A review on applications and challenges. *Remote Sensing Applications: Society and Environment*, *10*, 36–46. https://doi.org/10.1016/j.rsase.2018.02.005

Tooth, S., & Nanson, G. C. (2000). The role of vegetation in the formation of anabranching channels in an ephemeral river, Northern plains, arid central Australia. *Hydrological Processes*, *14*(16–17), 3099–3117. https://doi.org/10.1002/1099-1085(200011/12)14:16/17<3099::aid-hyp136>3.0.co;2-4

van Wesenbeeck, B. K., Van De Koppel, J., Mj Herman, P., & Bouma, T. J. (2008). Does scale-dependent feedback explain spatial complexity in salt-marsh ecosystems? *Oikos*, *117*(1), 152–159. https://doi.org/10.1111/j.2007.0030-1299.16245.x

Västilä, K., & Järvelä, J. (2014). Modeling the flow resistance of woody vegetation using physically based properties of the foliage and stem. *Water Resources Research*, *50*(1), 229–245. https://doi.org/10.1002/2013wr013819

Vincenot, C. E., Cartenì, F., Bonanomi, G., Mazzoleni, S., & Giannino, F. (2017). Plant–soil negative feedback explains vegetation dynamics and patterns at multiple scales. *Oikos*, *126*(9), 1319–1328. https://doi.org/10.1111/oik.04149

Vogel, S. (1989). Drag and reconfiguration of broad leaves in high winds. *Journal of Experimental Botany*, *40*(8), 941–948. https://doi.org/10.1093/jxb/40.8.941

Wang, X., Wang, W., & Zhang, G. (2017). Vegetation pattern formation of a water-biomass model. *Communications in Nonlinear Science and Numerical Simulation*, *42*, 571–584. https://doi.org/10.1016/j.cnsns.2016.06.008

Watson, K. J. (2007). *The seasonal influence of large aquatic plants at contrasting study sites on the River Frome, Dorset* (Unpublished doctoral dissertation). University of Nottingham.

Wharton, G., Cotton, J. A., Wotton, R. S., Bass, J. A., Heppell, C. M., Trimmer, M., et al. (2006). Macrophytes and suspension-feeding invertebrates modify flows and fine sediments in the Frome and Piddle catchments, Dorset (UK). *Journal of Hydrology*, *330*(1), 171–184. https://doi.org/10.1016/j.jhydrol.2006.04.034

Whiting, P. J., & Dietrich, W. E. (1990). Boundary shear stress and roughness over mobile alluvial beds. *Journal of Hydraulic Engineering*, *116*(12), 1495–1511. https://doi.org/10.1061/(asce)0733-9429(1990)116:12(1495)